



NKS-374  
ISBN 978-87-7893-459-8

---

## A summary of studies on debris bed coolability and multi-dimensional flooding

Eveliina Takasuo

VTT Technical Research Centre of Finland Ltd

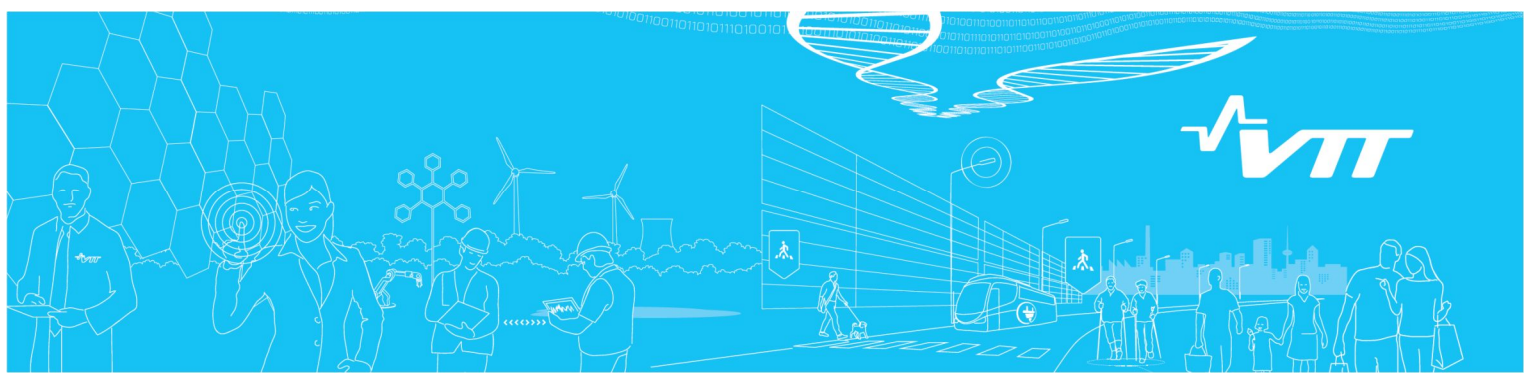
October 2016

## Abstract

A summary of the results of the experimental debris bed coolability studies in the COOLOCE programme at VTT is presented in this report. The experiments addressed the effects of the debris bed geometrical shape, which is a result of the melt jet fragmentation and solidification in a water pool. Six variations of the debris bed geometry with different flooding modes were examined in the experiments, including a top-flooded cylinder and five beds with more complex, heap-like geometries. Dryout heat fluxes of the different geometries and flooding modes were compared. In addition, the key question of transferring the experimental results and the small-scale simulations onto a reactor scale is briefly considered. A simulation case modelling a conically-shaped debris bed of 200 tonnes of corium in a generic containment geometry is presented. The large-scale simulation shows dryout characteristics similar to those of the earlier small-scale simulations of the experimental beds. The post-dryout behaviour of a multi-dimensionally flooded bed, which may reach steady-states even when local dryout has occurred, is clearly illustrated in the simulation.

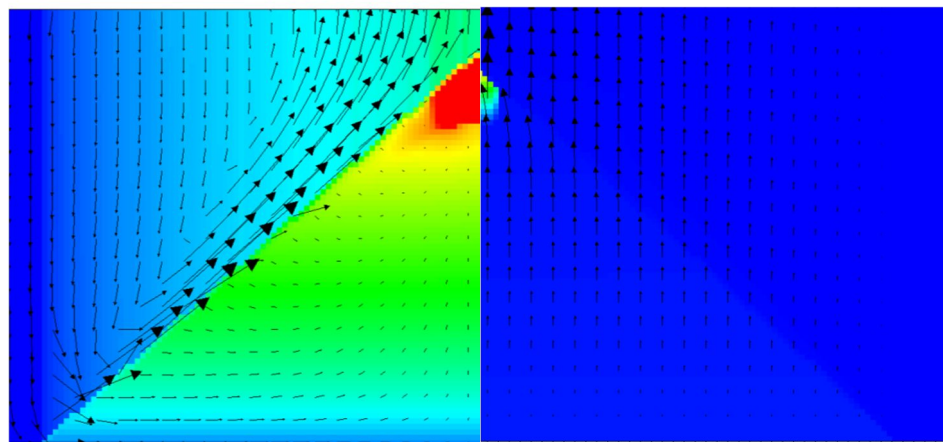
## Key words

nuclear reactor, severe accident, dryout heat flux, test facility, core debris, numerical simulation



## RESEARCH REPORT

VTT-R-00432-16

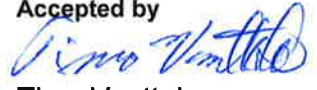


# A summary of studies on debris bed coolability and multi-dimensional flooding

Authors: Eveliina Takasuo

Confidentiality: Public

The views expressed in this document remain the responsibility of the author(s) and do not necessarily reflect those of NKS. In particular, neither NKS nor any other organization or body supporting NKS activities can be held responsible for the material presented in this report.

|   |  |
|---|--|
| <b>Report's title</b>   |  |
| A summary of studies on debris bed coolability and multi-dimensional flooding   |  |
| <b>Customer, contact person, address</b>  |  |
| SAFIR2018 Research Programme on Nuclear Power Plant Safety 2015 - 2018  | <b>Order reference</b><br>SAFIR 6/2015   |
| <b>Project name</b>   |  |
| Comprehensive Analysis of Severe Accidents  |  |
| <b>Author(s)</b>  |  |
| Eveliina Takasuo  | <b>Pages</b><br>27   |
| <b>Keywords</b>   |  |
| nuclear reactor, severe accident, dryout heat flux, test facility, core debris, numerical simulation  |  |
| <b>Summary</b>  |  |
| <p>A summary of the results of the experimental debris bed coolability studies in the COOLOCE programme at VTT is presented in this report. The experiments addressed the effects of the debris bed geometrical shape, which is a result of the melt jet fragmentation and solidification in a water pool. Six variations of the debris bed geometry with different flooding modes were examined in the experiments, including a top-flooded cylinder and five beds with more complex, heap-like geometries. Dryout heat fluxes of the different geometries and flooding modes were compared. In addition, the key question of transferring the experimental results and the small-scale simulations onto a reactor scale is briefly considered. A simulation case modelling a conically-shaped debris bed of 200 tonnes of corium in a generic containment geometry is presented. The large-scale simulation shows dryout characteristics similar to those of the earlier small-scale simulations of the experimental beds. The post-dryout behaviour of a multi-dimensionally flooded bed, which may reach steady-states even when local dryout has occurred, is clearly illustrated in the simulation.</p> |  |
| <b>Confidentiality</b>  |  |
| Public  |  |
| Espoo 23.2.2016   |  |
| <b>Written by</b><br><br>Eveliina Takasuo<br>Senior Scientist  | <b>Reviewed by</b><br><br>Anna Nieminen<br>Research Scientist |
| <b>Accepted by</b><br><br>Timo Vanttola<br>Head of Research Area   |  |
| <b>VTT's contact address</b>  |  |
| PO Box 1000, 02044-VTT, Finland   |  |
| <b>Distribution (customer and VTT)</b>  |  |
| SAFIR2018 Reference Group 2   |  |
| <i>The use of the name of VTT Technical Research Centre of Finland Ltd in advertising or publishing of a part of this report is only permissible with written authorisation from VTT Technical Research Centre of Finland Ltd.</i>  |  |

## Preface

---

The studies described in this report build on the continuous activities conducted in the frameworks of the SAFIR2014 (2011–2014) and SAFIR2018 (2015–) national programmes on nuclear power plant safety. Financially smaller but otherwise very significant contribution has been received from the NKS network in the form of the DECOSE project, conducted in collaboration with KTH. So far, the work on the COOLOCE experiments and simulations has produced one doctoral dissertation (in 2015), four journal papers (one of them is in press and two are joint papers), three scientific conference papers presented by the author, various contributions to joint conference papers, a couple of presentations to post-graduate students and – if my notes are on track – fourteen research institute reports.

Several technicians, engineers, research scientists and team leaders have participated to the work and made it possible for me to turn the low-budget sub-task of a SAFIR project into a productive experimental programme. Among the main contributors at VTT were Tuomo Kinnunen, Taru Lehtikuusi, Stefan Holmström, Pekka H. Pankakoski, Ville Hovi, Veikko Taivassalo and Mikko Ilvonen, who have all acted as my co-authors in the aforementioned publications and reports.

As the present report mainly focuses on summarizing the experimental data, it does not contain details of the work in previous publications. To readers interested in the parts of the work which are not included here, I would suggest to see my recent DSc thesis and the other publications, found in the reference list in the end of the report.

Esboo, 2.2.2016

The author

## Contents

---

|  |    |
|--|----|
| Preface.....   | 2  |
| Contents.....  | 3  |
| 1. Introduction .....                                | 4  |
| 2. Coolability experiments .....                     | 5  |
| 2.1 Debris bed shape variations.....                 | 5  |
| 2.2 Test facility.....                               | 6  |
| 2.3 Particle size and porosity .....                 | 8  |
| 2.4 Dryout determination.....                        | 10 |
| 2.5 Results .....                                    | 11 |
| 2.5.1 Heat flux in conical and cylindrical beds..... | 11 |
| 2.5.2 Dryout locations .....                         | 14 |
| 2.5.3 Effect of bed height .....                     | 16 |
| 2.5.4 Post-dryout conditions.....                    | 18 |
| 2.6 Measurement error and uncertainties .....        | 19 |
| 3. Simulations .....                                 | 20 |
| 3.1 Background and scaling.....                      | 20 |
| 3.2 Results .....                                    | 21 |
| 3.3 Discussion .....                                 | 24 |
| 4. Conclusions .....                                 | 24 |
| References.....                                      | 25 |

## 1. Introduction

---

One of the most important questions in the management of a severe nuclear reactor accident is how to cool and stabilize the molten corium. In a postulated severe accident at a Nordic-type BWR, the corium is discharged from the reactor pressure vessel into a deep water pool in the cavity below the RPV, which is called the lower drywell. The lower drywell is flooded by operator action prior to the RPV rupture. Then, the corium is discharged into the water pool where it is fragmented and solidified. After the initial quenching in the pool, a porous (ex-vessel) debris bed is formed on the floor of the containment. The debris bed continues to produce decay heat in the water pool, the power of which is great enough to result in remelting of the debris and a potential threat to the containment structures, unless it is effectively transferred from the debris. Sufficiently large heat removal rate is achieved by boiling the water in the pool. Then, the key question is how to ensure that an adequate amount of water may infiltrate into the debris bed to replace the evaporated coolant.

Numerous studies on debris coolability are found in the scientific literature, ranging from the fundamental studies in the early 80s (e.g. Trenberth and Stevens, 1980; Barleon and Werle, 1981; Lipinski, 1982; Hofmann, 1984) to more recent and still on-going research efforts that account for more complex conditions (e.g. Konovalikhin, 2001; Atkhen and Berthoud, 2006; Rashid et al., 2008; Repetto et al., 2011; Li et al., 2012). In addition to experimental work, the development and validation of different types of models to predict dryout has been a topic of significant interest (e.g. Bürger et al., 2006; Kudinov et al., 2014). Most of the debris coolability experiments have been performed in pipe-like set-ups in which the bed is flooded either through its top or bottom surface. These types of set-ups, designed for effectively one-dimensional flows, offer a very limited possibility to examine the effect of multi-dimensional flooding. Moreover, the realistic debris bed geometry is not considered at all in classical analyses. If the debris bed has a heap-like shape, complex multi-dimensional flow of coolant into the debris bed is possible. The geometry of the debris bed may determine whether the debris bed is coolable or not through the flooding mode.

The heap-shaped geometry can be considered as realistic based on fuel-coolant interaction experiments, in which such shapes have been formed as a result of the settling of melt particles (Spencer et al., 1994; Karbojian et al., 2009). This is a plausible assumption also because the pouring of granular material on a planar surface tends to form a conical heap. Experimental data on the coolability of heap-shaped debris beds, however, was practically non-existent prior to the COOLOCE test programme at VTT in 2011–2014. The tests were conducted in the frameworks of the SAFIR2014 and SAFIR2014 national programmes and the NKS-DECOSE project. The experiments consisted of dryout power and dryout heat flux (DHF) measurements for six variations of the debris bed geometry, including conical and heap-shaped beds. One of the geometries was a classical top-flooded bed to which the DHFs in the other geometries were compared. The objective was to reveal which types of geometries are favourable for coolability and which are less so. In addition, a main objective was to provide a basis for the validation of simulation codes that are used to assess severe accident scenarios on a reactor scale.

Modelling and numerical simulations have been an integral part of the debris coolability studies. The approach chosen at VTT was to use the MEWA 2D code developed by Stuttgart University (Bürger et al., 2006; Rahman, 2013), and to complement the MEWA results with detailed simulations using CFD. The applied CFD codes were ANSYS Fluent and the in-house two-phase flow solver PORFLO. Both 2D and 3D simulations were performed as has been reported previously in SAFIR and/or NKS reports (Takasuo et al., 2014, 2015). The goal of the 3D simulations was to develop the capability to assess non-symmetric and possibly highly irregular beds, and to scope the uncertainties related to the models and the typical assumptions made in the simulations. For instance, it was examined whether a free-flow model for the water pool affects the results and should be included in simulations. A doctoral dissertation completed in 2015 (Takasuo, 2015) includes the assessment of the

simulation results against the COOLOCE experiments, and gives guidelines on utilizing the experiments in code validation.

In this report, we first present the results of the geometry variation experiments and summarize them. The purpose of this is to provide a document in which the different COOLOCE results may be found “in one place”, making them more readily available for code validation or other scientific activities. In the second part, the key question of transferring the experimental results and the small-scale simulations onto a reactor scale is investigated. A simulation case modelling a debris bed of 200 tonnes of corium in a generic containment geometry is presented.

## **2. Coolability experiments**

---

### **2.1 Debris bed shape variations**

In many previous studies, the coolability increase caused by multi-dimensional flooding has been emphasized. The increased coolability is a result of the change in the two-phase flow pattern: in multi-dimensional flooding, co-current flow of steam and water may be formed in the debris bed – pool system, while in top-flooding, the flow is purely counter-current. The co-current flow has more cooling potential since, in this mode, the upwards flow of steam does not prevent the water from accessing the bed when the counter-current flow limitation at a critical steam generation rate is met. Instead, dryout is seen only when the steam generation is great enough to fully replace water in a bed cross-section.

In the present geometry studies, the dimensions of the debris bed were taken into account, instead of dealing only with the flooding mode differences. If the debris bed has a heap-like (conical) geometry, it is greater in height than a flat-shaped and top-flooded bed. The height allows the accumulation of a great local steam flux in the top parts of the bed, which makes this location vulnerable to dryout. For a bed with lower height, the maximum steam flux at the top is smaller, if the volumetric heat generation is the same. When realistic geometries are considered, it is not sufficient to consider only the flooding mode (top flooding vs. multi-dimensional), but also the bed height has to be accounted for.

In this work, the flooding modes are divided to top flooding, lateral flooding and multi-dimensional flooding. Principal sketches of the debris bed geometries and flooding modes addressed in the experiments are illustrated in Figure 1. In the case of a conical bed in Figure 1(a), the flooding mode is multi-dimensional because water can infiltrate into the porous bed through the full surface of the cone. The cylindrical bed with closed walls in Figure 1(b) is top-flooded because only the top surface is permeable to fluid flow. Lateral flooding applies to the geometry that has an impermeable top but open sidewall in Figure 1(d). Heap-shaped beds shown in Figures 1 (a) and (f) can be formed in the corium discharge and settling if the particles are not effectively spread by the flows in the water pool. The bed in Figure 1(c) is also a variation of the heap-like shape, since it is flooded though all surfaces, except the bottom. It is also possible that the debris settles partially against the wall while the top part of the bed has a conical shape, which is represented by the bed in Figure 1(e). The cylinder with lateral flooding and an impermeable top represents a case in which a layer of solid but non-fragmented corium has been formed on an otherwise heap-like bed.

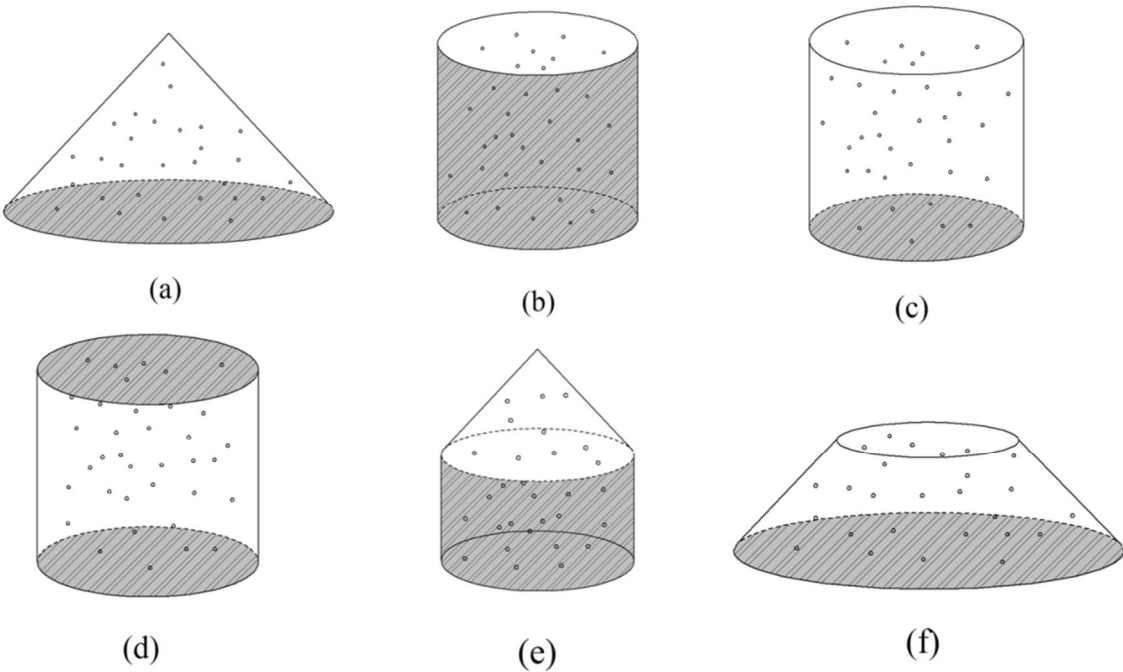


*Figure 1. Test bed geometry variations:(a) conical, (b) top-flooded cylinder, (c) fully-flooded cylinder (open walls), (d) cylinder with lateral flooding, (e) cone on a cylindrical base, and (f) truncated cone. The shaded areas are impermeable walls; other surfaces are permeable.*

It is important to note that the debris bed properties depend on the melt discharge process, the properties of which (e.g. melt jet diameter) depend on the in-vessel progression of the accident and the RPV failure mechanism. The chain of events leading to the formation of the porous bed is highly complex, and it would be practically impossible to take all possible debris distributions into account in experimental studies, or even in numerical simulations. In addition, the melt discharge from the RPV, the droplet solidification and the particle settling are stochastic processes which always include some randomness. It is possible that the real, irregular debris bed is not axially symmetric and/or has non-homogenous internal structure. Here, the possible non-symmetry has not been taken into account to keep the number of tests reasonable. Also, the effects of internal non-homogeneity, for instance, regions of higher porosity in the bed, have not been addressed.

## 2.2 Test facility

The experiments were conducted using the COOLOCE test facility, which has a modifiable test section for experimenting with different test bed geometries. The test bed is housed in a stainless steel pressure vessel which has an outer diameter of 613 mm and a volume of 270 litres. The pressure vessel contains the pool in which the test bed is immersed during experiments. The internal heating is achieved by vertically oriented electrical cartridge heaters, inserted into the bed through tapered holes in the bottom of the pressure vessel. The temperature sensors used for dryout detection are installed into the porous bed between the heaters, and they are similarly connected through the bottom. In addition to the pressure vessel containing the test bed, the facility consists of feed water, steam removal and data acquisition systems.

Photographs of the test beds are shown in Figure 2. The volumes ( $V$ ) and diameters ( $d$ ) of the test beds are indicated in the figure. The height of all test beds is 270 mm with the exception of the truncated cone, the height of which is 160 mm. The slope angle of the cone, the truncated cone and the top part of the cone on a cylindrical base is 47°. The conical bed has 137 heaters (6 mm in diameter) and 68 thermocouples (3 mm in diameter) at different heights. Viewed from the pressure vessel bottom, the heaters are installed into a "square mesh" at a distance of 30 mm from each other. The cylindrical bed has 69 heaters and 60 TCs. Depending on the experiment, one to three of the TCs were multi-point thermocouples that had ten sensor points at different elevations. The heating and thermocouple arrangements in the cylindrical bed are shown in Figure 3.

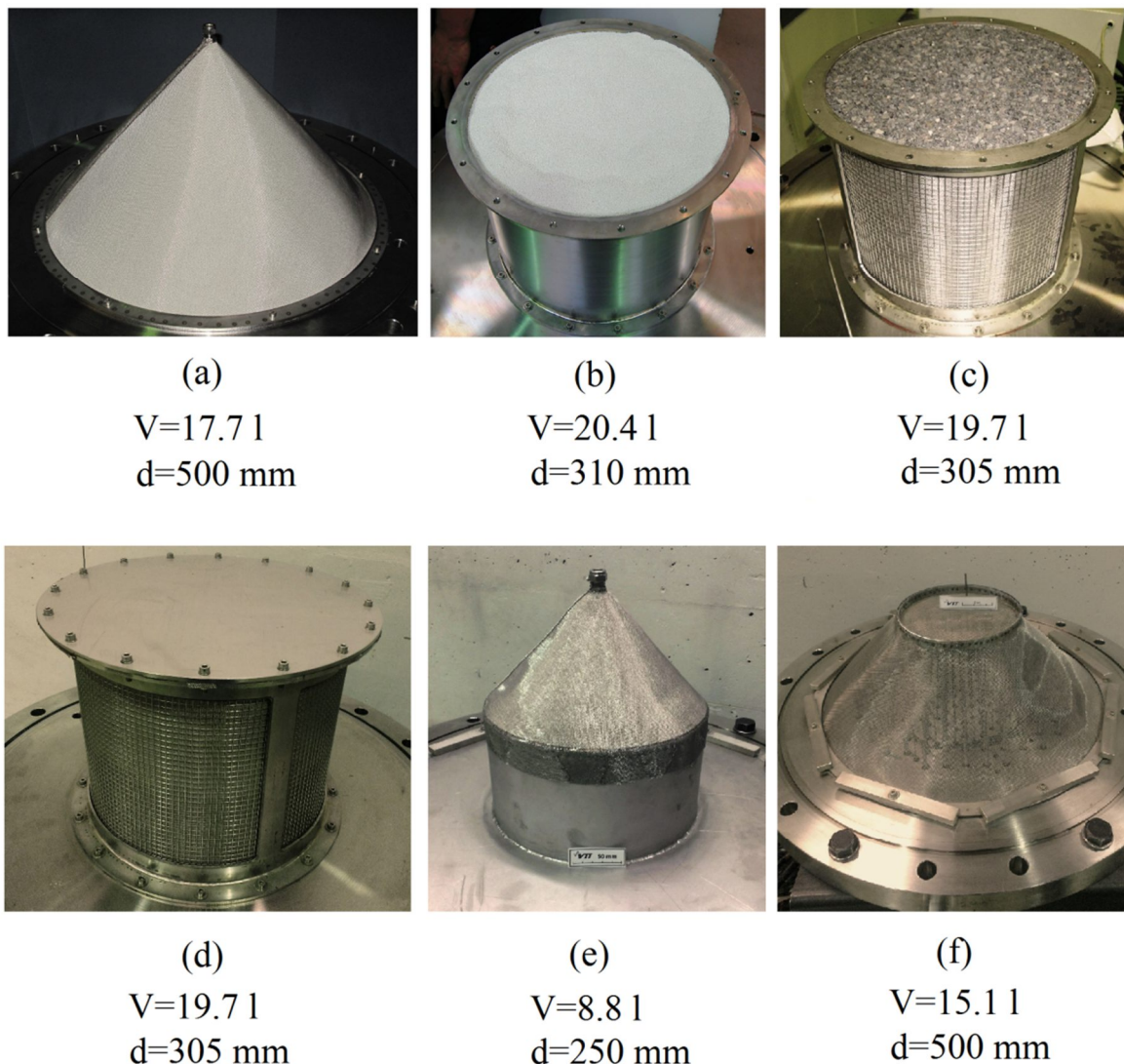


*Figure 2. The COOLOCE test beds: (a) conical, (b) top-flooded cylinder, (c) fully-flooded cylinder (open walls), (d) cylinder with lateral flooding, (e) cone on a cylindrical base, and (f) truncated cone.*

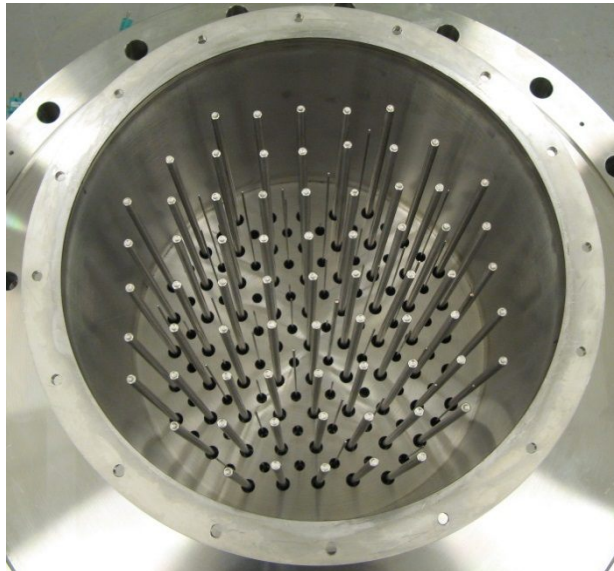


Figure 3. Heating and thermocouple arrangement of the cylindrical test bed.

The conical bed and the truncated cone that approximates a round-shaped heap are representative of reactor scenarios. The top-flooded cylinder is also a prototypic form, presuming that the debris is evenly spread in a flat layer. The fully flooded cylinder which allows water infiltration through all surfaces (except the bottom) is an approximation of the heap-shaped bed. This test bed was modified from the top-flooded bed by replacing the steel cylinder containing the test bed with a wire net. Later, it was decided to equip the fully conical arrangement with shorter heaters to achieve the truncated cone geometry. The cone on a cylindrical base considers the case in which the bottom part of the debris is spread evenly but the top part retains the conical shape. This combination shape is also possible in a reactor scenario, though the width-to-height ratio would be larger on a realistic scale.

The experiment with the laterally flooded cylinder having an impermeable top was motivated by the possibility of particle agglomeration. Partially molten particles may attach to each other to form agglomerates impermeable to fluid flow. Even large regions of solid "cakes" have been observed in experiments (Kudinov et al., 2013). It must be stated that a cake region that would fully cover the top of the debris bed is not a particularly probable configuration. However, its advantage compared to some completely arbitrary form of agglomerate is that it gives clearly defined conditions for experimentally testing the lateral flooding and evaluating the capabilities of simulation models to predict the dryout behaviour if flow in the lateral direction is dominating.

## 2.3 Particle size and porosity

The test beds were filled with ceramic beads (a mixture of  $Zr_2O_3$  and  $Si_2O_3$ ), used as the debris simulant material. The size of the beads was measured to be in the range of 0.815–1.126 mm by image processing analysis of a sample of 1000 particles. The arithmetic mean diameter was 0.97 mm. The size distribution was further verified by a laser diffraction analyser (Malvern, 2015), which showed results close to the image analysis. Even though the size distribution is narrow, different weighted averages for the particle size have been determined as a part of assessing the hydrodynamically and thermally representative, effective particle diameter (Chikhi et al., 2014). The weighted averages range from 0.97 mm (count mean) to 0.983 mm (mass mean). The maximum power output of the facility is about 55 kW, depending on the test bed, which means that experiments cannot be conducted with particles much larger than this because the dryout power may exceed the maximum power.

The porosity of the test beds was estimated by weighting the particles when building the test beds. For the top-flooded cylinder, porosity was also measured by filling the ready test bed with water and measuring the water volume. The porosities of the different test beds and experiments are listed in Table 1. The volumes of the heaters and TCs, which is approximately 2% of the total volume, are subtracted from the total volume in the porosity estimates.

For the truncated cone, the measured porosity of 0.354 is so low that the value is probably erroneous. The maximum random packing density of spherical particles corresponds to a porosity of about 0.366 (Song et al., 2008). The small porosity might be due to the stretching of the wire net, which would increase the amount of particles that can be fitted into the test bed. The wire net is a flexible structure, which means that the dimensions of the test beds supported by the net are more uncertain than those of the top-flooded cylinder constrained by a solid wall. For analytical purposes, it is reasonable to assume that the porosity of the truncated cone is approximately the same as the conical bed porosity (0.400). The measurement by filling the cylindrical test bed with water yielded a somewhat smaller porosity, 0.381.

The pressure range in which the experiments were performed is also given in the Table 1. There is some variation in the maximum pressure because in a number of cases the dryout power was greater than the maximum power of the facility (mainly in the higher pressures). The pressure range of 1–7 bar is considered as representative of the pressures expected in the containment of a Finnish BWR (Olkiluoto 1 and 2) in a postulated severe accident. The pressure increase is limited by the filtered venting of the containment.

*Table 1. List of the geometry experiments, including bed porosities and test pressures.*

| Experiment    | Geometry  | Porosity | Pressure (bar) |
|---------------|---|----------|----------------|
| COOLOCE-3 – 5 | Cylindrical, top flooding                                 | 0.390    | 1.1–7.0        |
| COOLOCE-6 – 7 | Conical, multi-dimensional flooding                       | 0.400    | 1.1–3.0        |
| COOLOCE-10    | Cylindrical, lateral and top flooding                     | 0.392    | 1.3–2.9        |
| COOLOCE-11    | Cylindrical, lateral flooding                             | 0.392    | 1.1–6.9        |
| COOLOCE-12    | Cone on a cylindrical base, flooding through conical part | 0.375    | 1.1–3.8        |
| COOLOCE-13    | Truncated cone, multi-dimensional flooding                | 0.354*   | 1.3            |

\*Probably too low (due to error in bed dimensions).

In addition to the experiments in Table 1, the test programme included series numbered COOLOCE-1–2, -8 and 9. COOLOCE-8 was conducted with alumina gravel to obtain comparison data for the experiments with the ceramic beads. COOLOCE-9 was conducted with initially subcooled water in order to scope the effect of the pool subcooling that might be expected in the case of a real accident (Takasuo, 2015, pp. 59–61). The first tests, COOLOCE-1–2, were preliminary experiments with the conical test bed, the results of which are not considered as reliable as those from the later experiments because the temperature

increase indicating dryout was not very clear and measurements above 2 bar pressure were not successful. The repeatability of the measured dryout power was verified by one additional measurement in three test set-ups, COOLOCE-3, -4 and -8. The results of the first and the repeated experiments differed by less than 1 kW. The test beds were not disassembled and re-packed between the measurements.

## 2.4 Dryout determination

The test runs are started with a heat-up sequence during which the facility is pressurized and the temperature is increased up to the saturation temperature (at the pressure of the intended experiment) and steady-state boiling is developed. The heat-up sequence is followed by the test sequence which consists of stepwise increases of heating power until temperature excursion from the saturation temperature is indicated by one or more of the temperature sensors installed into the test bed. This indicates dryout at the sensor location(s). To allow the development of dryout, a waiting time of 20–30 minutes is applied at each power level, between the power steps.

The result of the measurement is a pair of powers: the maximum power at which the bed is in a coolable steady state and the minimum power at which local dryout is reached. The minimum power at which local dryout is reached is taken as the dryout power, and the corresponding heat flux is the dryout heat flux (DHF). The heat flux corresponding to the maximum coolable power is denoted CHF. The size of the power steps was 1–2 kW and the measured dryout power varied between 15–55 kW. The maximum operating temperature in the experiments was about 165°C, which is the saturation temperature at 7 bar.

Due to technical reasons, there is variation in the test bed volumes (see Figure 2). Thus, the total dryout power ( $W$ ) which is recorded by the data acquisition system is not a very useful variable for comparing the flooding effectiveness, because it depends on the volume. Power density ( $W/m^3$ ) is more useful in assessing the relative coolability because it is independent of the dimensions. Dryout heat flux ( $W/m^2$ ) is practical for comparing the flooding effectiveness because, for a homogenously heated bed, it is independent of the bed height. Here, the flooding mode comparisons are presented using the dryout heat flux at the top boundary of the bed.

The heat flux  $q$  at the top boundary of the bed can be calculated by multiplying the power density  $Q$  ( $W/m^3$ ) by the bed height  $z$  (m), which equals to the total power  $P$  ( $W$ ) divided by the surface area  $A$  ( $m^2$ ) of the bed top:

$$q = Qz = \frac{P}{A} \quad (1)$$

It is important to note that, if a conical and a cylindrical geometry are equal in volume and radius, the cone is three times higher than the cylinder (since the volume of the cone is  $1/3 \cdot \pi \cdot r^2 \cdot z$ ). Then, if the two geometries have the same power density, the heat flux at the top of the cone is three times that of the cylinder. The effect of the test bed height is treated separately by converting the dryout heat fluxes measured for the top-flooded cylinder back to power density. The independence of DHF from the bed height makes this comparison possible so that the "absolute" heat removal capabilities (in  $W/m^3$ ) of the flat-shaped cylindrical bed and the tall, conical beds may be compared.

It is expected that the multi-dimensional flooding facilitated by the conical shape of the bed increases the dryout power and coolability compared to the flat, top-flooded cylinder, but the increased height counteracts this effect because it facilitates the formation of greater heat flux near the top of the bed. When considering the coolability in realistic containment geometries, the dimensions of the debris bed cannot be ignored.

The heat flux represents the enthalpy of the steam flow that exits from the bed, averaged over the cross-sectional surface area. The heat flux is by definition a surface-related variable, which is directly applicable only for one-dimensional flow in which the steam flow is directed upwards. In the conical bed, no top surface exists that would be directly comparable to that of the cylinder. However, the heat flux at the highest point of the cone and other geometries illustrated in Figure 1 can be calculated with Equation 1 using the power density. For the heat flux comparisons, it makes no difference whether the highest point of the geometry, for which the maximum heat flux is calculated, is a point or a planar surface. The effectiveness of the different geometry-related flooding modes can easily be compared by comparing the DHFs at the maximum height of the bed, without considering the surface areas.

## 2.5 Results

### 2.5.1 Heat flux in conical and cylindrical beds

The dryout heat fluxes for the six geometry variations are collected in Figure 4. The heat fluxes are arranged according to the geometry, and the pressure of the experiment is shown on the x-axis. The DHF and CHF on the chart indicate the minimum dryout heat flux and the maximum coolable heat flux, respectively. The zone marked with lighter colour at the top of the bars indicates the difference between the measured DHF and CHF. This is the measurement error caused by the power steps in the dryout detection.

The most informative pressure levels are 1 bar and 2 bar because, above these pressures, the dryout power gradually became greater than the maximum output of the facility for most geometries. At 5–7 bar only two measurements were possible (with the two beds that had the poorest coolability). The measured dryout power (in kW) for each experiment is presented in Table 2, which also shows the dryout power density (in kW/m<sup>3</sup>), calculated from the dryout power and the test bed volume (shown in Figure 2). The rightmost column of the table shows the ratio DHF/DHF<sub>0</sub> where DHF<sub>0</sub> is the dryout heat flux of the top-flooded cylinder. This coolability ratio describes the effectiveness of the flooding mode in comparison to the classical geometry: the top-flooded cylinder.

The greatest DHFs and the best relative coolability were obtained for the cone on a cylindrical base, the fully-flooded cylinder and the fully conical bed, and also for the truncated cone. The DHF/DHF<sub>0</sub> ratios for these geometries were 1.47–1.93. At the pressures of 2 bar and 3 bar, the ratio was 1.50–1.73. The experiment with the cone on a cylindrical base that showed the ratio of 1.93 has a large error margin due to the large final power step in the experiment, but the CHF in this experiment is almost equal to that of the fully flooded cylinder. By ruling out the probably exaggerated DHF, it can be concluded that the coolability increase for the cases with multi-dimensional flooding and permeable top surfaces is 47–73% compared to top-flooding only.

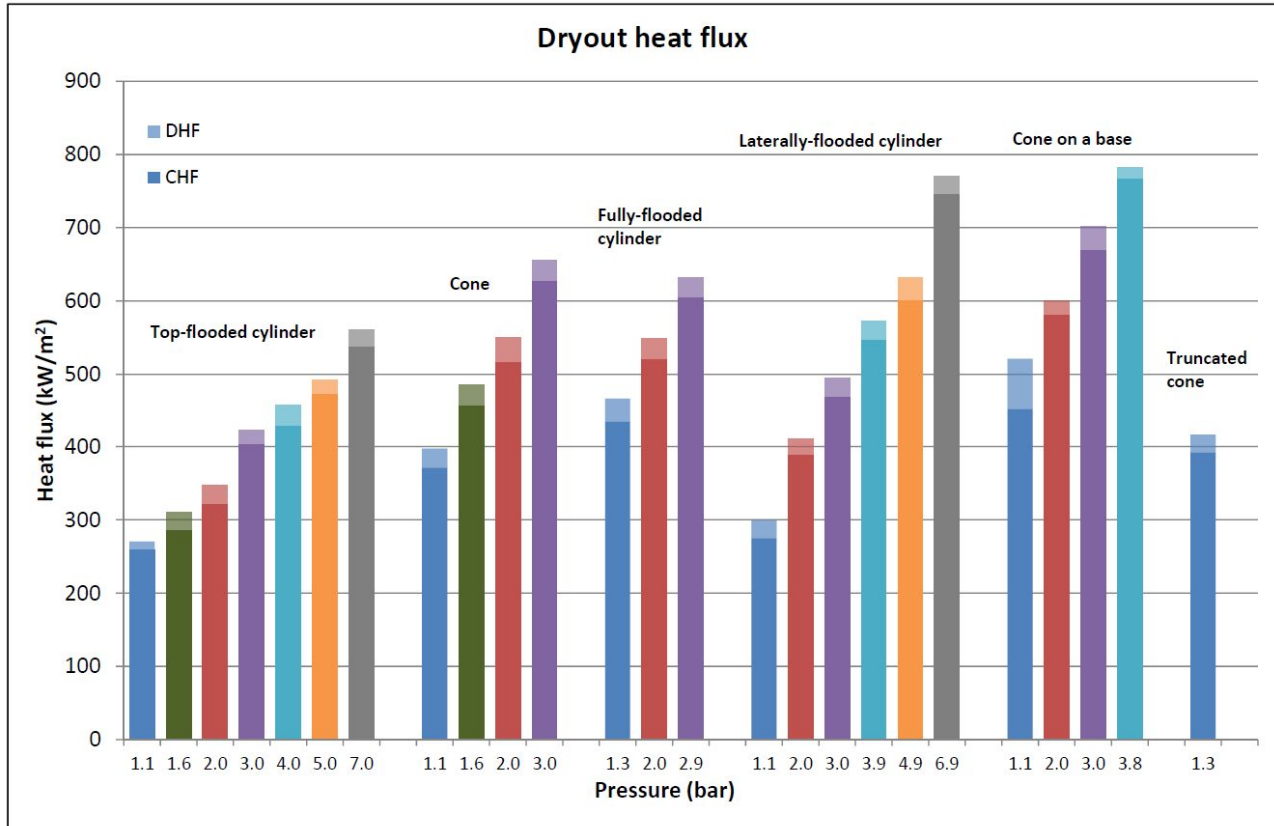


*Figure 4. The dryout heat fluxes (DHF) in the COOLOCE experiments for the different geometries and pressures. CHF is the maximum coolable power and the zone with lighter colour at the top is the error margin DHF-CHF.*

Common to the four geometries with high DHF is that some form of multi-dimensional infiltration of water is present: water can flood the bed through lateral surfaces to replace steam, which exits upwards through the top of the bed. The lowest dryout heat fluxes were seen for the top-flooded cylinder and the cylinder with lateral flooding only. In the case of the top-flooded cylinder, the reduced coolability is explained by the fact that the two phases have to flow in counter-current mode: water can infiltrate only through the top surface against the upwards flowing steam.

In the case of the laterally flooded cylinder which has a solid top plate, both water and steam have to infiltrate and exit through the open lateral surface. The top plate forces the steam to escape through the side of the bed instead of the top surface, which makes the top part below the plate vulnerable to dryout. The DHF/DHF<sub>0</sub> ratio shows that the cylinder with lateral flooding only is almost equally inefficient in removing the heat than the top-flooded cylinder. For pressures above atmospheric, the cylinder with the top plate has greater DHF than the top-flooded cylinder, with the DHF/DHF<sub>0</sub> ratio of 1.17–1.37, which increases as a function of pressure. It must be mentioned that this result might be sensitive to the thickness of the unheated layer of about 40 mm below the top plate. If the heating would reach the top plate and TCs were located there, the DHF of this geometry might be smaller, because even a thin layer of steam accumulated under the top plate would be detectable.

Table 2. Results of the debris bed geometry experiments.

| Test bed                                   | Pressure (bar) | Dryout power (kW) | Power density (kW/m <sup>3</sup> ) | DHF (kW/m <sup>2</sup> ) | DHF/DHF <sub>0</sub> |
|--|----------------|-------------------|------------------------------------|--------------------------|----------------------|
| Top-flooded bed                            | 1.10           | 20.4              | 1001                               | 270                      | 1.00                 |
|  | 1.60           | 23.4              | 1148                               | 310                      |                      |
|  | 2.00           | 26.2              | 1286                               | 347                      |                      |
|  | 3.00           | 31.9              | 1565                               | 423                      |                      |
|  | 4.00           | 34.6              | 1698                               | 458                      |                      |
|  | 5.00           | 37.2              | 1825                               | 493                      |                      |
|  | 7.00           | 42.3              | 2076                               | 560                      |                      |
| Conical bed                                | 1.10           | 26                | 1471                               | 397                      | 1.47                 |
|  | 1.60           | 31.8              | 1800                               | 486                      | 1.57                 |
|  | 2.00           | 36                | 2037                               | 550                      | 1.58                 |
|  | 3.00           | 42.9              | 2428                               | 655                      | 1.55                 |
| Fully-flooded bed                          | 1.30           | 34.1              | 1729                               | 467                      | 1.73                 |
|  | 2.00           | 40.1              | 2033                               | 549                      | 1.58                 |
|  | 2.90           | 46.2              | 2342                               | 632                      | 1.50                 |
| Laterally-flooded bed with impermeable top | 1.10           | 21.9              | 1110                               | 300                      | 1.11                 |
|  | 2.00           | 30                | 1521                               | 411                      | 1.18                 |
|  | 3.00           | 36.2              | 1835                               | 495                      | 1.17                 |
|  | 3.90           | 41.8              | 2119                               | 572                      | 1.25                 |
|  | 4.90           | 46.2              | 2342                               | 632                      | 1.28                 |
|  | 6.90           | 56.3              | 2854                               | 771                      | 1.37                 |
| Cone on a cylindrical base                 | 1.09           | 17.1              | 1930                               | 521                      | 1.93                 |
|  | 1.98           | 19.7              | 2224                               | 600                      | 1.73                 |
|  | 2.95           | 23.0              | 2597                               | 701                      | 1.66                 |
|  | 3.81           | 25.6              | 2896                               | 782                      | 1.71                 |
| Truncated cone                             | 1.25           | 39.2              | 2602                               | 416                      | 1.54                 |

An interesting observation is that the best coolability was found for the combination flooding: the cone on a cylindrical base. At 1 bar level, the error due to the size of the power step was large but the trend of this geometry having the greatest DHF (as well as CHF) continues systematically up to 4 bar pressure. Apparently, the dryout behaviour is governed by flooding through the conical part in this geometry. The mass flux of steam accumulated in the outer — and the lowest — region of the test bed does not prevent water from infiltrating to the bottom of the bed through this region. Concerning the dryout zone, it is not important whether the bottom region of the test bed receives coolant through the inclined surface of the full cone, or through the flow downwards near the perimeter of the cylindrical part in the cone on a base. Both geometries are capable of providing water into the bottom region. This explains why the cone on a base configuration has as good coolability as the fully conical bed, but not why it should be even better coolable.

Taking into account that the DHF/DHF<sub>0</sub> ratio of 1.93 at atmospheric pressure is probably too high, the general difference between the results is rather small (DHF/DHF<sub>0</sub> above 1 bar is 1.66–1.73). Then, possible causes of the large measured DHF in the cone on a cylindrical base might be related to the slightly different volumetric distribution of heating power, minor

differences in the packing of the material, or even inaccuracies in the test bed dimensions which affect volume in the calculation of the heat flux (and porosity as mentioned in Section 2.3). Note that the total power required to reach the dryout heat flux is smaller for the cone on a base test bed than for the fully conical and cylindrical beds due to the smaller size (width) of the test bed. This made it possible to achieve dryout at 4 bar while, for the other well coolable geometries the maximum was 3 bar, and only 1 bar for the truncated cone.

Experiments at atmospheric pressure had more pressure fluctuations than experiments with a pressurized test vessel. This was because the pressure cannot be controlled in the normal manner when the steam line valve, which is used for pressure control, is fully open and the large steam flow rate out of the pressure vessel tends to build counter-pressure in the pipe line. This resulted in the dryout pressures for the fully-flooded cylinder and the truncated cone being greater by 0.15–0.2 bar than in the other experiments, in which the average pressure at the dryout power was 1.1 bar. This explains the relatively high DHF for the fully-flooded cylinder at 1.1 bar (1.73 DHF/DHF<sub>0</sub> ratio) while, for greater pressures, the DHF for this geometry is practically equal to that of the conical geometry. For the truncated cone, no high-pressure comparison data exists, but the elevated pressure suggests that the DHF also for this geometry is slightly too high. The increase of DHF with pressure is a well-known phenomenon, which is mainly caused by the increased steam density, resulting in smaller void fractions in the bed at constant power. The steam density at 1 bar is about 0.6 kg/m<sup>3</sup> and 3.7 kg/m<sup>3</sup> at 7 bar.

## 2.5.2 Dryout locations

In addition to the DHFs, the measured locations of the incipient dryout are of interest since they yield information about the dryout mechanisms. The dryout locations are illustrated in Figure 5 by the red areas, which indicate successfully measured dryout points, including all pressure levels for the test bed shown. The locations are approximate and based on the temperature sensor data. Dryouts were not measured in the centre of the test bed in the radial direction because this location is occupied by a heating cartridge. The innermost TCs are at 21.2 mm distance from the centre point.

It was found that the two variations of the cylindrical bed, the fully flooded and the laterally flooded bed, and the truncated cone dried out near the top. The cone on a cylindrical base developed dryout above the junction of the conical and cylindrical parts (upper central region). The fully conical bed also showed dryout in the upper central region, with some variation depending on the test run. The top-flooded bed indicated dryout in the lower central part. In the radial direction, dryouts were near the center of the test bed, not near the perimeter: the sensors, with which dryout was monitored, were at 21.2 mm or 48.5 mm from the bed centre.

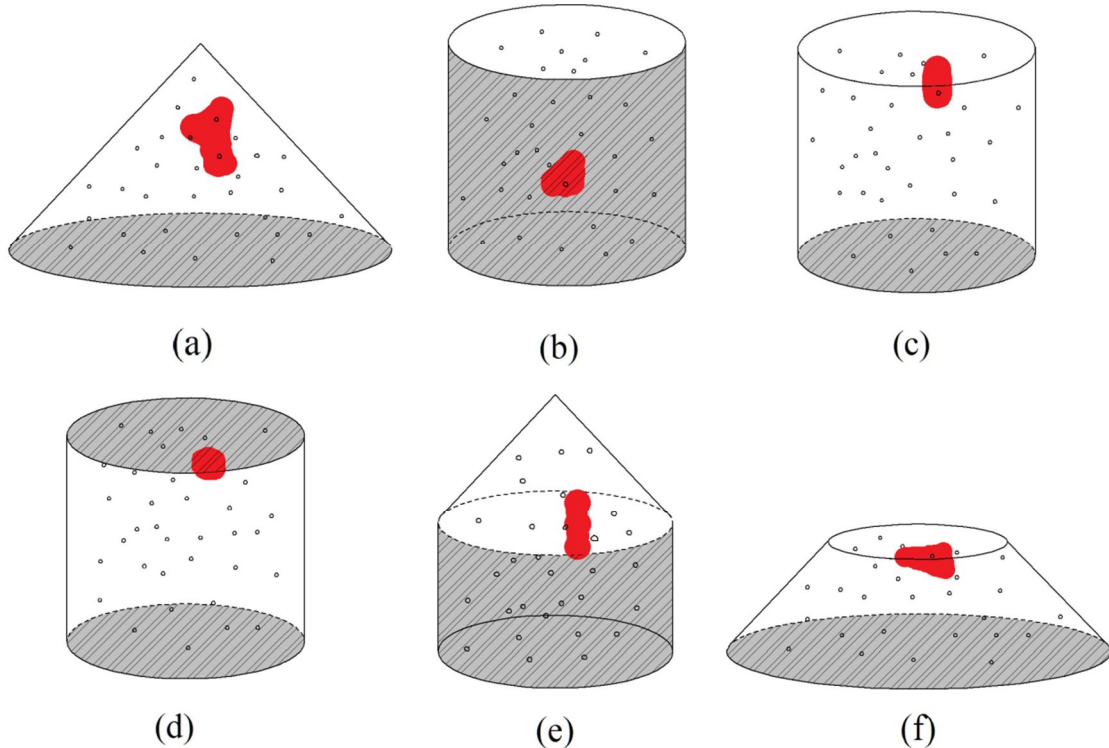


*Figure 5. Approximate dryout locations in the experiments (all measurements for each geometry are shown).*

In a previous publication (Takasuo et al., 2012a), the dryout locations of the fully conical bed and the top-flooded cylinder are compared to the locations predicted by a 2D simulation model. In the model predictions, dryout was formed in the tip of the cone and in the bottom of the cylinder. This is in accordance with several publications addressing the dryout in top-flooded and conical beds, though for the conical beds, the data before the present study was obtained from numerical simulations, not from experiments (Hofmann, 1984; Ma, 2011; Sehgal, 2012, p. 341). It must be mentioned that in the previous publication (Takasuo et al., 2012a) the given percentage of the dryout volume to the total bed volume in the conical and cylindrical bed experiments is erroneously stated as 4-20%. The correct percentage is 0.4-2%.

The dryout locations found in the experiments are not reproduced in the simulations in detail. This is because, firstly, capturing the exact dryout power would need a measurement with almost infinite accuracy and, secondly, because the internal non-homogeneity of the test beds causes 3D effects not present in the debris bed model. Homogenous heating is usually applied in the simulation models, imitating the internally heated particles of realistic debris beds. In experimental set-ups, it is difficult to achieve homogeneous internal heating. Because of the vertical orientation of the heaters, which probably causes preferential flow paths for steam in the vicinity of the heaters (a result of increased porosity next to the heater surface), it cannot be expected that the simulations and the experiments would be in exact agreement, in terms of void fractions and temperatures. In most of the experiments, no spreading of dryout was seen. For the top-flooded cylinder, the absence of spreading is probably due to the heating and TC arrangement which favours local dryout.

It is important to note that dryout is not measured near the heater surfaces: the temperatures are recorded in the porous medium between the heaters, where the TCs are located (the thin rods in Figure 3). The sensors may also cause preferential flow paths (channelling) since

their orientation is vertical, but there is no heating at the TC surfaces. There is some evidence (presently non-conclusive) that the COOLOCE facility might exaggerate the dryout power and coolability due to its heating and sensor arrangement, which was observed by comparing the top-flooding DHFs measured with COOLOCE facility to the DHFs measured with the POMEKO-HT facility at the Royal Institute of Technology (Takasuo, 2015, pp. 80–81). The channelling is not expected to influence the DHF/DHF<sub>0</sub> ratios since the possible effect is expected to be similar in all geometries.

### 2.5.3 Effect of bed height

The examination of the coolability problem on a realistic scale requires that the dimensions of the debris beds are accounted for. The conical geometry is three times higher than the cylindrical one if the volumes and radii are equal (with the assumption that the bed is spread to cover the floor of the spreading area in both cases). The flat-shaped cylindrical bed is flooded only through the top surface, since it is limited by the walls of the containment. Note that the same debris mass and porosity is also assumed for the beds. For the 270 mm conical test bed, the height of the flat-shaped cylinder would be 90 mm, as illustrated in Figure 6.

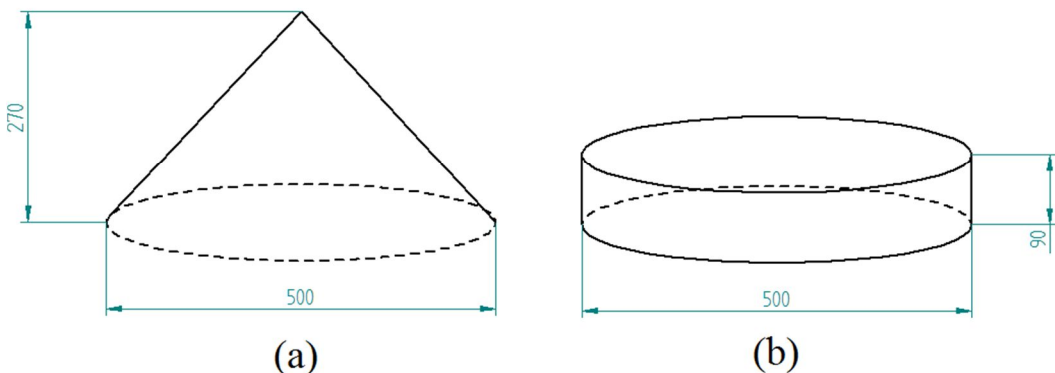
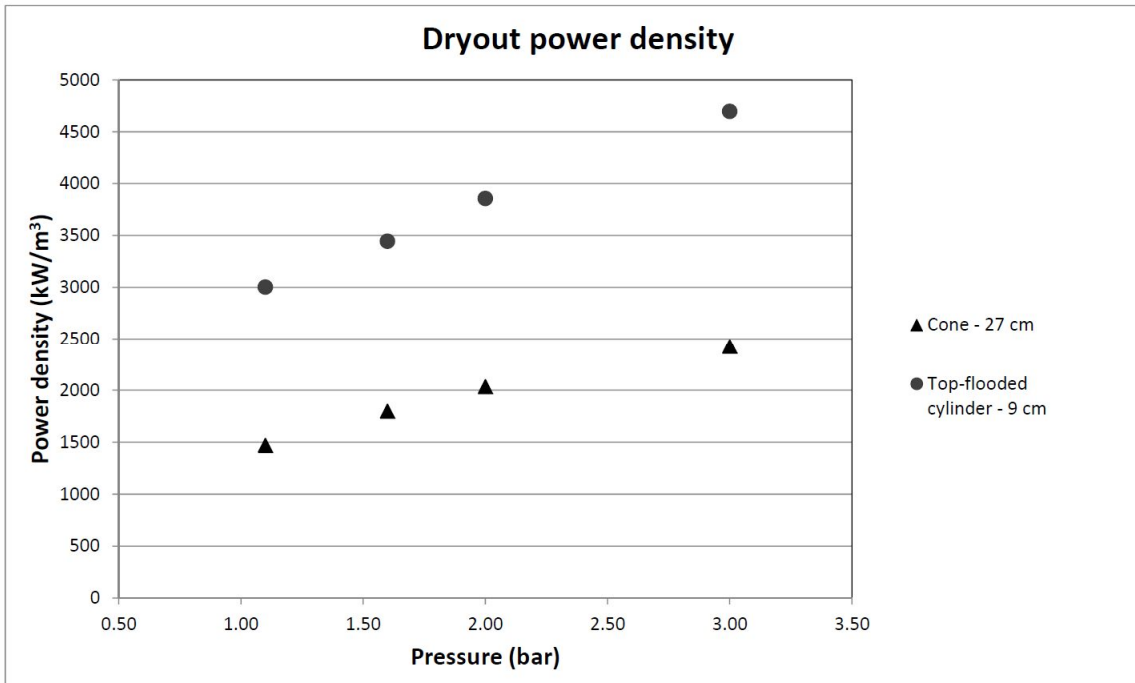


Figure 6. (a) Conical and (b) cylindrical beds of equal volume and radius.

Figure 7 shows the dryout power density for the beds in Figure 6. The power density is calculated from Equation 1 by inserting the dryout heat fluxes reported in the previous section and the heights of 270 mm and 90 mm into the equation. For the conical bed, the calculation yields the power densities reported in Table 2 but, for the cylindrical bed, the height is scaled down to 90 mm. This means that the power density for the flat bed must increase in order to meet the dryout heat flux.

It is seen that the dryout power density is greater for the cylindrical bed at all pressures by 89–100%. The total power that would be required for dryout in a 90 mm cylinder increases by the same ratio because the volumes are assumed to be equal. It is clear that the benefit achieved by the multi-dimensional flooding is not sufficient to compensate for the effect of the increased height. According to the experiments, DHF increases of coarsely 50–60% can be achieved with multi-dimensional flooding, but the heat flux increase at the top boundary of the examined conical bed is 200%. The DHF/DHF<sub>0</sub> ratio represents a limit for the debris bed height: if the heap-shaped bed is more than 1.5–1.6 times higher than the top-flooded bed, the benefit from the multi-dimensional flooding is lost.



*Figure 7. Dryout power densities as a function of pressure for the conical test bed and the flat-shaped cylinder.*

Because the dryout heat flux simply describes the heat flow through a surface — or through a point as described in Section 2.4 — it is not very useful for describing the coolability of beds with multi-dimensional flooding. Therefore, the dryout heat flux should not be used as a direct measure of coolability, unless the bed is flooded one-dimensionally. For reactor scenarios, it is much more illustrative to compare the dryout power (in W) to the total decay power generated by the debris bed. Alternatively, power density ( $\text{W}/\text{m}^3$ ) or specific power ( $\text{W}/\text{kg}$ ) can be used. The present study can be seen to consist of two approaches to the coolability problem. First, the dryout heat fluxes were compared in order to find out the effect of the flooding mode on dryout heat fluxes. Secondly, the dryout heat fluxes were used to calculate to power density and total power for beds of different heights.

The reason for not directly measuring the dryout power of a 90 mm cylinder was that this test bed would have been impractically low, even to the extent of possibly causing notable boundary layer effects between the pool and the bed, and would have required too high heating power compared to the capacity of the facility. (In addition, this approach would have hidden the effect of the flooding mode, similarly to the effect of the bed height being “hidden” in the present experiments, because of test beds of equal height.)

The other geometries of the COOLOCE experiments are not easily scalable to the reactor scenario due to the varying width-to-height ratios and the multi-dimensional flooding. Nevertheless, the effect of the bed height was clearly observed in certain other experiments. In the case of the truncated cone, the DHF was coarsely the same as that of the conical and fully-flooded beds, but the power density and total power required for dryout were notably higher. The fully conical bed showed dryout at about  $1470 \text{ kW}/\text{m}^3$  and  $26.0 \text{ kW}$  at  $1.1 \text{ bar}$  but the truncated cone required  $2601 \text{ kW}/\text{m}^3$  at  $1.25 \text{ bar}$ , corresponding to  $39.2 \text{ kW}$ . This is a direct result of the bed height difference: the mass flux of steam, which is responsible of the dryout formation, increases with the bed height. For the truncated cone, the power generation has to be great enough to yield the dryout mass flux (heat flux) in the distance of 160 mm, whereas for the conical bed, the “available” distance is 270 mm. Taking into account the pressure uncertainty, the measured DHFs for the conical, fully-flooded and truncated beds were so close to each other that it can be concluded that the flooding modes

of these geometries are equally efficient. Consequently, the overall coolability of the heap-shaped beds with permeable tops depends on the bed height, which determines the maximum possible heat flux.

#### 2.5.4 Post-dryout conditions

From the point of view of overall coolability, and for considering which types of conditions can be stated as being safe, it is not sufficient to examine only the formation of local dryout. The characteristics of dryout in the multi-dimensionally flooded beds differ from those of one-dimensionally flooded beds, and this is true also for the post-dryout behavior. The multi-dimensionally flooded beds dry out near the top, where the dryout zone is initially very small and subjected to steam flow from the parts of the bed which remain saturated with water, as shown in studies applying simulation models (Takasuo et al., 2012a; Yakush and Kudinov, 2014). In these conditions, it is possible that the debris bed reaches a new steady state in which the temperature is stabilized, without the risk of reaching re-melting temperatures.

The post-dryout conditions are difficult to study experimentally, since this easily causes overheating and failure of the heaters. Some evidence of temperature stabilization was seen in the experiment with the truncated cone (COOLOCE-13R) in which the temperature at the dryout power stabilized at about 10°C above the saturation temperature. A further 2 kW (5%) increase resulted in an apparently continuous temperature increase. The temperature evolution in this experiment is illustrated in Figure 8.

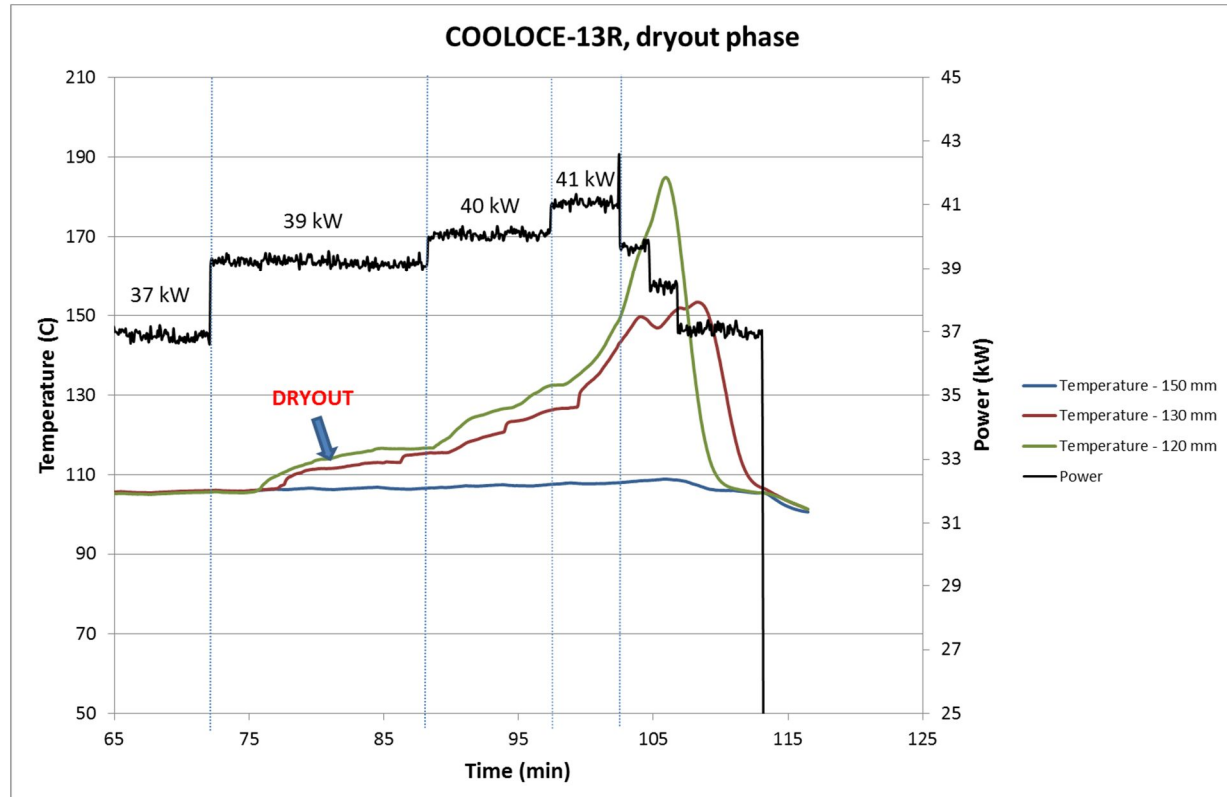


Figure 8. Temperature evolution in the truncated cone experiment, indicated by sensors at three different heights in the test bed (120, 130 and 150 mm, test bed height 160 mm). Heating power is shown on the secondary vertical axis.

It is an unanswered question why such post-dryout behaviour was not seen in the other COOLOCE experiments, but it must be stated that it is very difficult to interpret the temperature data measured in dryout conditions. This is because the experimental runs were usually terminated soon after verified dryout, without allowing time to observe whether temperatures would have stabilized, in order to avoid damage to the heaters. It is also possible that this type of behaviour is specific to the truncated cone test bed.

Greater steady-state temperatures have been reported in at least one other experimental study: in the SILFIDE experiments heated by an induction coil, temperature stabilization was seen for temperatures up to 200°C above the saturation temperature (Atkhen and Berthoud, 2006). The experimental evidence of post-dryout steady states is not comprehensive but it supports the simulations which are consistent in stating this phenomenon as favourable for achieving coolable conditions for the corium. In this case "coolable" refers to the limited increase of temperature, not to the loss of liquid water in the pores of the bed. It is worth considering defining the coolability limit using the solid temperature, rather than the void fraction because (1) the void fraction criterion may be overly conservative and (2) it is the high temperature that threatens the containment integrity, not the phase fraction.

## 2.6 Measurement error and uncertainties

The main source of error in the experiments is the power increase scheme. The exact dryout heat flux is between the reported DHF and CHF, which causes a relative error of 5–11% depending on the pressure. The accuracy of the power measurement is  $\pm 0.3$  kW for power levels up to 42 kW (applicable for most of the measurements). Above 42 kW, the error is larger, being about  $\pm 0.6$  kW for 50 kW power level. This error estimate includes the voltage conversion error and calibration inaccuracy. The power does not remain completely stable throughout the experiments, and small power fluctuations depending on e.g. the temperature dependence of the heater resistivity were seen. The reported dryout power values are power step averages that have been cross-checked against the values shown by the power analyser display.

The accuracy of the pressure control is about  $\pm 0.1$  bar. Pressure fluctuations occurred during the test runs due to the insertion of cooler feed water (80°C), in addition to the difficulties in maintaining the vessel unpressurized during some of the 1 bar experiments. The nominal accuracy of the thermocouples is 1.5°C. The sensor-specific accuracy against the saturation temperature has been checked during the test runs, and the fluctuations have been very small (a few tenths of a °C). The temperature closely followed the pressure fluctuations. The thermocouple error is not assumed to contribute to the dryout power measurement since dryout is registered only after a clear and sustained temperature increase of at least a few degrees, which cannot be confused with small fluctuations.

It has been acknowledged that the vertical orientation of the heaters and TCs can result in unintended channelling of the flows in the bed due to the increased porosity near the surface of the vertical structures. The effect of the local heating and the increased porosity near the heater surfaces on the measured dryout power is too complicated to be accounted for with normal error estimation. However, because the main objective was to study the differences in the flooding mode and all the experiments were planned to be conducted with similar heating arrangement, this is not considered to be an issue that would reduce the comparability of the results. In addition, the temperature sensors for dryout detection are located in the porous medium between the heaters, not next to the heater surfaces where the possible local effects are realised.

In some of the experiments (particularly in COOLOCE-3–5 and -6–7), the average condensate mass flow at the steam line exit was estimated by weighing the condensed

water. The average power and DHF were calculated from the mass flow rate by assuming that the flow rate equals to the evaporation rate by the heated test bed. The power obtained this way was lower than the control power reported in the previous sections by 7–20%. This is due to the heat losses from the facility, the energy consumed by heating the subcooled feed water, and the possible direct contact condensation in the vessel when the cooler feed water mixed into the water pool is in contact with the evaporating steam. The difference between the power calculated from the condensate mass and the control power is largest at the high pressure levels. This is explained by the increased heat losses to the environment and the increased subcooling of the feed water (the saturation temperature increases but the feed water from the pre-heater is at about 80°C). It was estimated that the heating of the feed water to the saturation temperature is the main source of the deviation between the control power and the estimated evaporation power.

The heat losses are not considered to influence the comparative coolability of the different geometries (DHF/DHF<sub>0</sub> ratios). However, the observed difference between the two powers introduce an uncertainty to the absolute value of DHF. As a consequence, the measured CHFs and DHFs may be greater than what they would be in a completely isolated test arrangement in thermal equilibrium in saturated conditions. It was mentioned in Section 2.5.2 that the COOLOCE facility was found to exaggerate the DHF in comparison to the POMEKO-HT facility, which is a pipe-like test facility and has horizontally-oriented heaters. The difference unexplained by differences in porosity or pressure was about 20% (Takasuo et al., 2014). This comparison, however, did not consider the power calculated from the condensate flow. If compared to the power calculated from the condensate mass flow, the COOLOCE results would be closer to the POMEKO-HT results. Thus, the difference in the measurements between the two facilities may not only be related to the heating arrangement but also to the greater heat losses in the COOLOCE facility, or other less obvious differences in the test set-ups.

### 3. Simulations

---

#### 3.1 Background and scaling

The geometry variation experiments have been modelled by using the MEWA 2D code (formerly WABE) developed by the IKE Institute at Stuttgart University as described in previous reports (Takasuo et al. 2014; Takasuo, Hovi, et al. 2012; Takasuo 2013). The simulations have included all the pressure levels in the tests, as well as several variations of porosity and particle size to address the uncertainties related to these key parameters, which have a large effect on the particle-fluid drag forces and, thus, on the dryout heat flux.

The main difference between MEWA and the two other codes applied in the studies, namely PORFLO and Fluent, which are referred to as CFD codes, is that MEWA solves a simplified version of the momentum equations, which consists of a relation between the pressure gradient and the different drag force components (Schmidt, 2004; Rahman, 2013). In the CFD codes, the full momentum equation with the viscous stress term, the convection term and the time derivatives is solved. The set of simulation cases calculated with PORFLO and Fluent is not as extensive as that of MEWA, because the CFD simulations are longer (computationally expensive) and their application includes a considerable amount of in-house development work. The doctoral dissertation by Takasuo (2015) includes the general conclusions of the simulation work.

In principle, the scaling of a top-flooded test bed to the realistic scale is rather straightforward. This is because there is no need to take the lateral distance travelled by the fluid into account, and there are no velocity, pressure or temperature gradients in the radial direction. However, this is not the case in the multi-dimensional flooding mode. In case of the

COOLOCE test beds, the height and width are both smaller compared to the reactor scale. The conical test bed is about 1:7 in height and 1:18 in diameter compared to a debris bed of about 200 000 kg of corium and 40% porosity. On a realistic scale, the angle of repose in the conical test bed is smaller due to the lower height-to-width ratio: For a conical debris bed whose base reaches the walls of the spreading area, the angle of repose would be approximately 22° while the angle in the COOLOCE test bed is 47°.

The steam generation in the realistic debris as a whole is, of course, greater than in the test bed. The effect of the height may be examined using the Reynolds number, which depends on the flow velocity  $v$  (m/s), particle size  $d_p$  (m), density  $\rho$  (kg/m<sup>3</sup>) and viscosity  $\mu$  (Pa·s).

$$Re = \frac{|\rho \vec{v} d_p|}{\mu} \quad (2)$$

Keeping in mind that the steam flux increases with height and power density, the steam phase achieves greater velocity in a real debris bed compared to the test bed. With greater flow velocity and the same particle size, the Reynolds number increases, which suggests that the steam flow is more turbulent. In the simulation models, the momentum equation for both gas and liquid is closed by models based on the famous Ergun's equation (Ergun, 1952), representing drag forces between the fluids and the solid. For the gas phase, the solid-fluid drag  $\overrightarrow{F}_{s,g}$  (N/m<sup>3</sup>) is

$$\overrightarrow{F}_{s,g} = \varepsilon \alpha \left( \frac{\mu_g}{KK_{rg}} \overrightarrow{J}_g + \frac{\rho_g}{\eta \eta_{r,g}} |\overrightarrow{J}_g| \overrightarrow{J}_g \right) \quad (3)$$

where  $\varepsilon$  is porosity (-),  $\alpha$  is the gas volume fraction (-),  $K$  (m<sup>2</sup>) is permeability,  $\eta$  (m) is passability and  $\overrightarrow{J}_g$  (m/s) is the superficial velocity of gas. The dimensionless factors  $K_{rg}$  and  $\eta_{rg}$  are the relative permeability and passability, the purpose of which is to account for the presence of the other phase (liquid) in the two-phase flow.

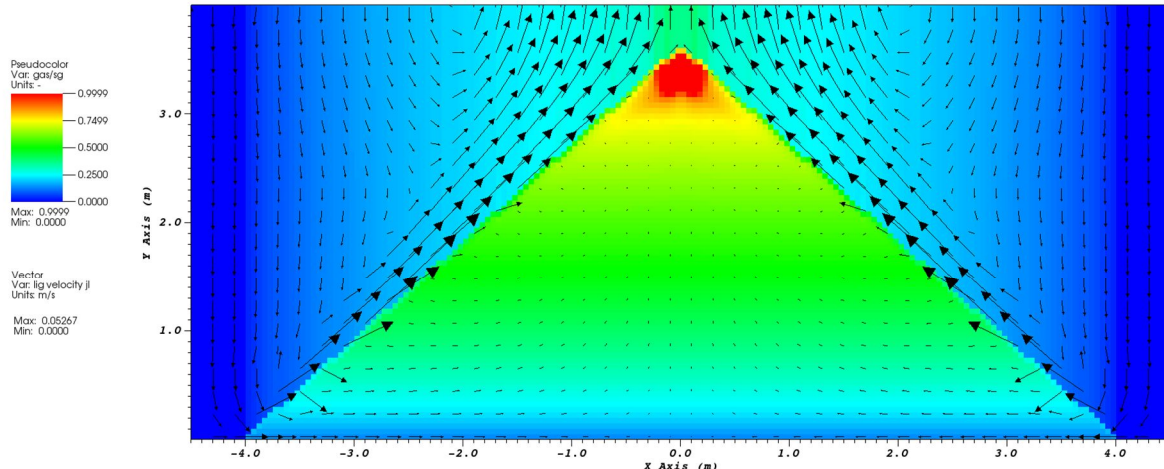
From the equation of the gas phase drag, it is seen that the inertial component (the last, quadratic component on the right) of the pressure loss is greater on the large scale than on the laboratory scale due to the velocity increase. This also suggests that the flow instabilities are greater. Note that the scale differences are pronounced in the upper parts of the bed where the length of the steam flow path is greatest. In principle, the simulation models are capable of taking this transition towards higher velocities into account.

One of the effects of the larger geometry is that the fluidization limit, at which the particles start to float in the fluid flow, is more easily reached due to the larger drag force. This might enhance the self-levelling of the bed, which acts towards increased coolability because it is expected to reduce the bed height. A more difficult question to answer is whether the different height-to-width ratio affects the effectiveness of the lateral flooding. There is no experimental data of multi-dimensional flooding in different scales, and it has to be assumed that the simulation models are adequate for capturing the main characteristics of the flow also on the reactor scale.

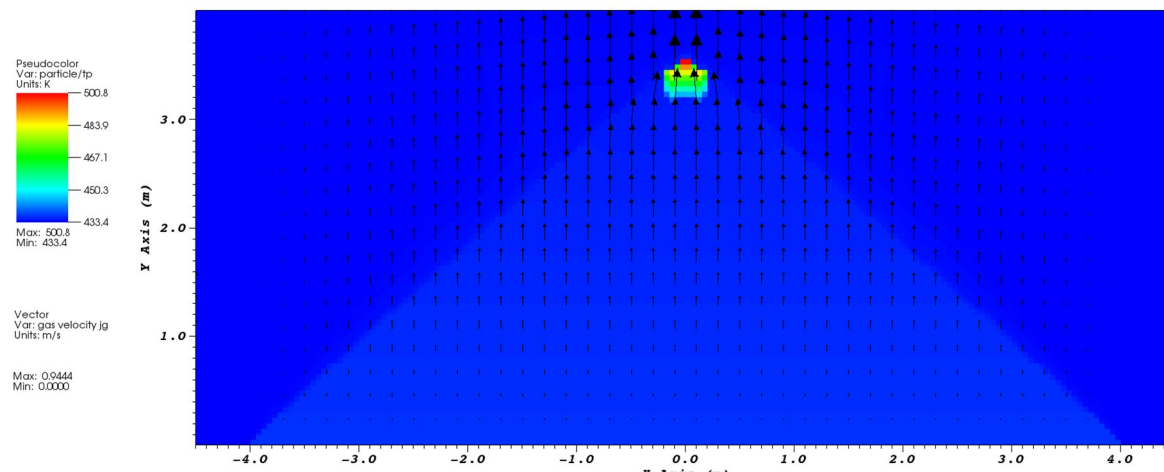
### 3.2 Results

A BWR calculation with MEWA is shown in Figure 9, which illustrates the void fraction and temperature distributions for a debris bed consisting of about 200 000 kg of solidified corium. The angle of repose has been conservatively set to 42° in order to create a tall, fully conical bed. The containment pressure in the simulation is 5.5 bar and the applied drag force model is the modified Tung and Dhir model. This model, which has been developed by the Stuttgart

University, includes an explicit consideration of the interfacial drag (Rahman, 2013). The decay power has been adjusted to just exceed the dryout power.



(a)



(b)

*Figure 9. (a) Void fraction and (b) solid temperature in a MEWA simulation of the conical debris bed on a realistic scale. The dryout power is just exceeded. Vectors of superficial velocity are shown in (a) for liquid and (b) for gas.*

It was seen that the general behaviour – the void fraction, the flow directions and the temperature map – was very similar to the simulation of the small-scale conical test bed. The steam flow is directed almost directly upwards, and the water flow forms a convection loop in which it travels laterally into the bed interior through the conical surface and turns upwards with the steam flow in the centre of the bed. The solid temperature has stabilized to 228°C, about 70 °C above the saturation temperature in the bottom of the pool. The results, especially the similar steam flow pattern, suggest that the coolability is strongly dependent on the bed height on the reactor scale.

The size of the dryout zone in the simulation of Figure 9 does not increase, and the temperature remains clearly below the re-melting temperature, unless the heating power is further increased. In the case of only a small increase, the system finds a new steady state

with greater solid temperature and slightly larger dryout zone size. This is shown in Figure 10, which illustrates the void fraction and solid temperature in the same simulation case as in Figure 9, with the heating power increased by 10%. Now, the solid temperature is stabilized at 289°C, which is still an order of magnitude smaller than the temperature of fully molten corium. For comparison, the melting point of uranium dioxide is approximately 2850°C (IAEA, 2006).

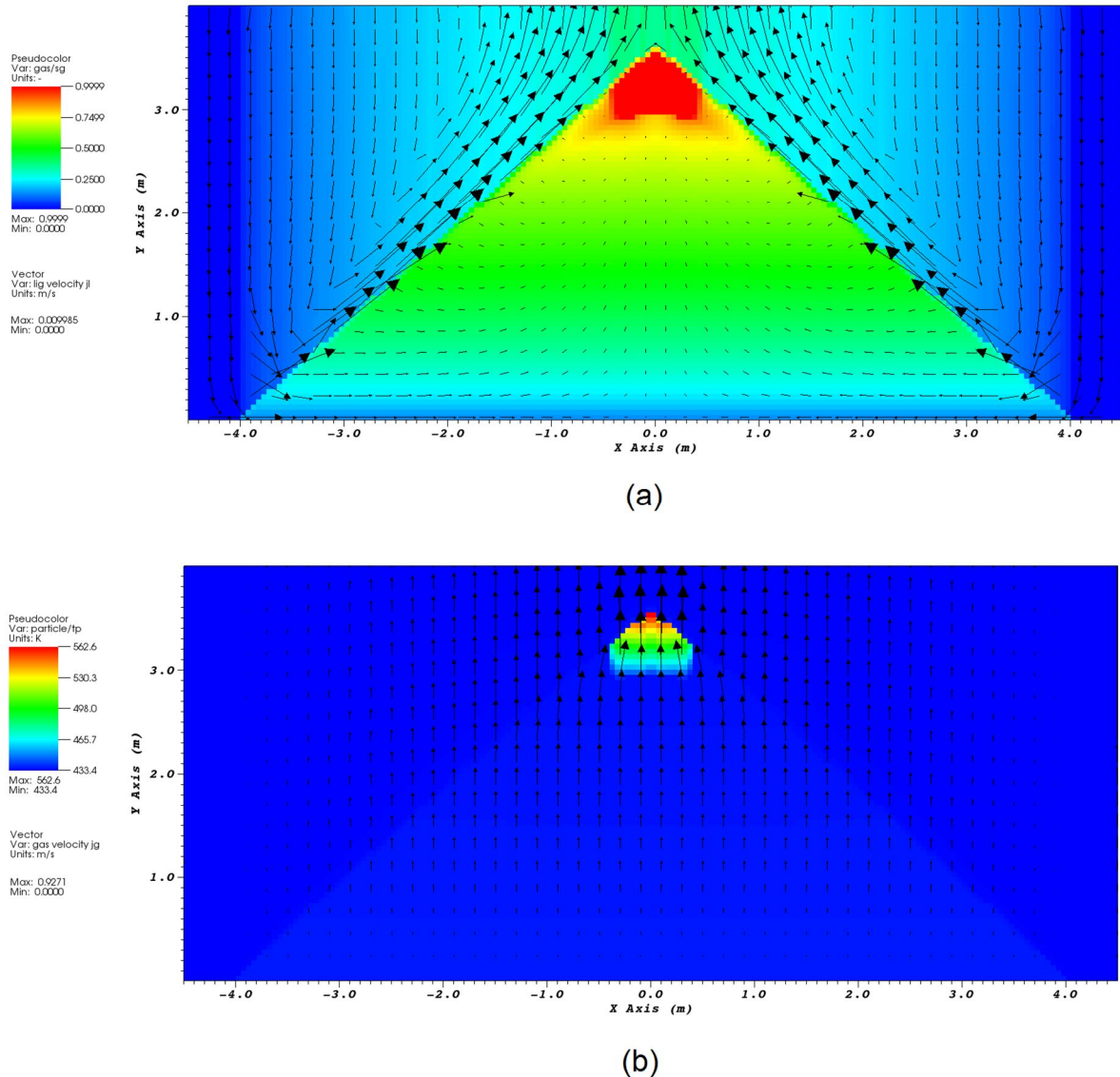


*Figure 10. (a) Void fraction and (b) solid temperature in a MEWA simulation of the conical debris bed on a realistic scale. The dryout power is exceeded by 10%. Vectors of superficial velocity are shown in (a) for liquid and (b) for gas.*

The co-current flooding pattern and the steam flow that passes through the dry zone cannot sustain the steady conditions if the heat generation is excessively high. When the power increases to a critical level, the convection by steam flow is no longer capable of removing the heat from the particles effectively and the temperature increases until the corium starts to re-melt. (Re-melting can result, for instance, in a molten pool lower in the bed, which is insulated from the surrounding debris by a solidified layer called crust.) A significant contributor to the loss of cooling by steam flow is the reduction in the evaporating steam flow

rate; when the size of the dry zone increases by spreading downwards, the water reservoir below the dry zone that provides the steam flow becomes smaller.

### 3.3 Discussion

The data available of the maximum excess power and the critical size of the dryout zone at which steady states can be formed are scarce. One of these studies conducted at KTH (Yakush and Kudinov, 2014) makes an effort to quantify the maximum permitted size of the dryout zone in a conical bed by using the DECOSIM code which, in general, utilizes an approach similar to MEWA. According to the study, the dryout zone might spread to cover more than 50% of the bed height until temperature stabilization is no longer possible. However, no experimental data exists to verify this single-phase cooling behaviour, at least in the context of experiments dedicated to severe accidents and debris coolability.

Concerning the modelling of heat transfer, the properties of the experimental material differ from that of corium (e.g. their thermal conductivity is lower). This may play a role in the behaviour of post-dryout temperatures, even though it is not apparent based on the simulations which apply realistic material properties for the corium. In addition, it should be pointed out that the validation of the heat transfer models for prediction of the post-dryout temperature increase is a topic which has not been reviewed in the current studies (since the focus has been on the DHF experiments and simulations). It is recommended to review the available heat transfer models and their validity in different configurations prior to the application of the temperature-based criterion for coolability.

In the dryout zones, adverse effects might also result from the exothermic reaction of zirconium oxidation at temperatures above 1000°C (IAEA, 2011). This reaction, which is responsible of the hydrogen generation in a severe accident, produces additional heat (and a source of hydrogen) that may have poorly predictable effects on the debris re-melting behavior. Then, the maximum "safe" temperature applied in coolability simulations could be based on the start of the high-temperature zirconium oxidation, instead of the onset of debris re-melting.

In any case, as already discussed in Section 2.5.4, the results suggest that it is reasonable to base the coolability limit on the temperature increase, rather than on the formation of the first dry zone (void fraction). In top-flooded beds, both criteria yield the same result, because dryout is followed by a remarkable temperature increase, as postulated e.g. by Schmidt (2004). For multi-dimensionally flooded beds, dryout is highly local, and the void-based coolability criterion is apparently overly conservative.

## 4. Conclusions

---

A summary of the results of experimental debris bed coolability studies at VTT has been presented. The focus was on the debris bed geometrical shape, and its effect on the dryout heat flux. Six variations of the debris bed geometry were included in the study, one of which was a top-flooded cylinder and five that had more complex geometries. The complex geometries included conical and heap-like beds which can be considered prototypic to reactor scenarios. The main difference between the top-flooded bed and the heap-shaped beds is that the heap-like shape allows multi-dimensional infiltration (flooding) of coolant into the bed interior.

The experiments show that multi-dimensional flooding increases the dryout heat flux compared to top flooding by 47-73%. For heap-like geometries, which include a conical bed

and a conical bed with flattened top, the increase was 47-58%. The results also suggest that the benefit from the multi-dimensional flooding is lost if the heap-shaped bed is more than about 1.5-1.6 times higher than the top-flooded bed. This is because the heat flux in the bed increases linearly as a function of height, making dryout possible at the top of a heap-shaped bed. Thus, the heap-like geometry has a twofold effect on coolability: it increases the dryout heat flux by facilitating multi-dimensional infiltration of water into the bed, but it also decreases the dryout power by having a greater height.

In addition to the experimental results, a simulation case of a conical bed in a BWR reactor has been presented. It was found out that, in general, the large-scale bed behaves similarly to the small-scale bed of the geometry variation experiments. With the simulation case, the post-dryout behaviour of the multi-dimensionally flooded bed was demonstrated. Even though dryout has been reached, the solid temperature in the dryout zone is clearly stabilized if the excess power is small (in this case 10%). This, among simulations conducted by other researchers, suggests that a temperature-based coolability criterion should be considered for multi-dimensionally flooded beds, instead of a void-based criterion.

## References

---

- Atkhen, K., Berthoud, G., 2006. SILFIDE experiment: Coolability in a volumetrically heated debris bed. *Nucl. Eng. Des.* 236, 2126–2134.
- Barleon, L., Werle, H., 1981. Dependence of Dryout Heat Flux on Particle Diameter for Volume- and Bottom-Heated Debris Beds. Tech. Report. Kernforschungszentrum Karlsruhe. KfK 3138.
- Bürger, M., Buck, M., Schmidt, W., Widmann, W., 2006. Validation and application of the WABE code: Investigations of constitutive laws and 2D effects on debris coolability. *Nucl. Eng. Des.* 236, 2164–2188.
- Chikhi, N., Coindreau, O., Li, L.X., Ma, W.M., Taivassalo, V., Takasuo, E., Leininger, S., Kulenovic, R., Laurien, E., 2014. Evaluation of an effective diameter to study quenching and dry-out of complex debris bed. *Ann. Nucl. Energy* 74, 24–41.  
doi:10.1016/j.anucene.2014.05.009
- Ergun, S., 1952. Fluid Flow Through Packed Columns. *Chem. Eng. Prog.* 48, 89–94.
- Hofmann, G., 1984. On the location and mechanisms of dryout in top-fed and bottom-fed particulate beds. *Nucl. Technol.* 65, 36–45.
- IAEA, 2006. Thermophysical properties database of materials for light water reactors and heavy water reactors.
- IAEA, 2011. Mitigation of Hydrogen Hazards in Severe Accidents in Nuclear Power Plants.
- Karbojian, A., Ma, W.M., Kudinov, P., Dinh, T.N., 2009. A scoping study of debris bed formation in the DEFOR test facility. *Nucl. Eng. Des.* 239, 1653–1659.
- Konovalikhin, M.J., 2001. Investigations on Melt Spreading and Coolability in a LWR Severe Accident. Royal Institute of Technology. PhD thesis.
- Kudinov, P., Karbojian, A., Tran, C.-T., Villanueva, W., 2013. Agglomeration and size distribution of debris in DEFOR-Experiments with Bi<sub>2</sub>O<sub>3</sub>--WO<sub>3</sub> corium simulant. *Nucl. Eng. Des.* 263, 284–295.
- Kudinov, P., Konovalenko, A., Grishchenko, D., Yakush, S., Basso, S., Lubchenko, N., Karbojian, A., 2014. Analysis of Debris Bed Formation, Spreading, Coolability, and

- Steam Explosion in Nordic BWRs Nordic Nuclear Safety Research. NKS-317.
- Li, L., Ma, W., Thakre, S., 2012. An experimental study on pressure drop and dryout heat flux of two-phase flow in packed beds of multi-sized and irregular particles. *Nucl. Eng. Des.* 242, 369–378.
- Lipinski, R.J., 1982. A Model for Boiling and Dryout in Particle Beds. US Nuclear Regulatory Commission, NUREG/CR-2646.
- Ma, W., 2011. Prediction of Dryout Heat Flux of Volumetrically Heated Particulate Beds Packed with Multi-Size Particles, in: Nureth-14. pp. 1–11.
- Malvern, 2015. Mastersizer 3000. <http://www.malvern.com/en/products/product-range/mastersizer-range/mastersizer-3000/default.aspx>.
- Rahman, S., 2013. Coolability of Corium Debris under Severe Accident Conditions in Light Water Reactors. Institut für Kernenergetik und Energiesysteme, University of Stuttgart.
- Rashid, M., Chen, Y., Kulenovic, R., Laurien, E., 2008. Experiments on the coolability of a volumetrically heated particle bed with irregularly shaped particles, in: 7th International Meeting on Nuclear Reactor Thermal Hydraulics Operation and Safety, NUTHOS-7, Seoul, Korea, October 5–9, 2008.
- Repetto, G., Garcin, T., Eymery, S., Fichot, F., 2011. Experimental program on debris reflooding (PEARL) -- Results on PRELUDE facility. *Nucl. Eng. Des.* 264, 176–186.
- Schmidt, W., 2004. Influence of Multidimensionality and Interfacial Friction on the Coolability of Fragmented Corium. PhD Thesis. Institut für Kernenergetik und Energiesysteme, University of Stuttgart.
- Sehgal, B.R., 2012. Nuclear Safety in Light Water Reactors. Severe Accident Phenomenology. Elsevier.
- Song, C., Wang, P., Makse, H.A., 2008. A phase diagram for jammed matter. *Nature* 453, 629–632.
- Spencer, B.W., Wang, K., Blomquist, C.A., McUmber, L.M., Schneider, J.P., 1994. Fragmentation and Quench Behaviour of Corium Melt Streams in Water. US Nuclear Regulatory Commission, NUREG/CR-6133.
- Takasuo, E., 2013. Debris coolability simulations with different particle materials and comparisons to COOLOCE experiments.
- Takasuo, E., 2015. Coolability of porous core debris beds. Effects of bed geometry and multi-dimensional flooding. VTT Technical Research Centre of Finland Ltd. D.Sc. thesis. <http://www.vtt.fi/inf/pdf/science/2015/S108.pdf>.
- Takasuo, E., Holmström, S., Kinnunen, T., Pankakoski, P.H., 2012a. The COOLOCE experiments investigating the dryout power in debris beds of heap-like and cylindrical geometries. *Nucl. Eng. Des.* 250, 687–700. doi:10.1016/j.nucengdes.2012.06.015
- Takasuo, E., Hovi, V., Ilvonen, M., Holmström, S., 2012b. Modeling of Dryout in Core Debris Beds of Conical and Cylindrical Geometries, in: 20th International Conference on Nuclear Engineering Collocated with the ASME 2012 Power Conference. July 30–August 3, 2012, Anaheim, California, USA.
- Takasuo, E., Taivassalo, V., Hovi, V., 2014. A study on the coolability of debris bed geometry variations using 2D and 3D models. VTT Technical Research Centre of Finland. VTT-R-00676–14.
- Takasuo, E., Taivassalo, V., Kinnunen, T., Lehtikuusi, T., 2015. Coolability analyses of heap-shaped debris bed. VTT Technical Research Centre of Finland Ltd. VTT-R-00367-15.
- Trenberth, R., Stevens, G.F., 1980. An experimental study of boiling heat transfer and dryout

in heated particulate beds. UKAEA Atomic Energy Establishment, Winfrith.

Yakush, S., Kudinov, P., 2014. A model for prediction of maximum post-dryout temperature in decay-heated debris bed, in: 22nd International Conference on Nuclear Engineering. July 7-11, 2014, Prague, Czech Republic.

|                                  |  |
|----------------------------------|--|
| Title                            | A summary of studies on debris bed coolability and multi-dimensional flooding  |
| Author(s)                        | Eveliina Takasuo   |
| Affiliation(s)                   | VTT Technical Research Centre of Finland Ltd   |
| ISBN                             | 978-87-7893-459-8  |
| Date                             | October 2016   |
| Project                          | NKS-R / DECOSE   |
| No. of pages                     | 27   |
| No. of tables                    | 2  |
| No. of illustrations             | 10   |
| No. of references                | 31   |
| Abstract<br>max. 2000 characters | A summary of the results of the experimental debris bed coolability studies in the COOLOCE programme at VTT is presented in this report. The experiments addressed the effects of the debris bed geometrical shape, which is a result of the melt jet fragmentation and solidification in a water pool. Six variations of the debris bed geometry with different flooding modes were examined in the experiments, including a top-flooded cylinder and five beds with more complex, heap-like geometries. Dryout heat fluxes of the different geometries and flooding modes were compared. In addition, the key question of transferring the experimental results and the small-scale simulations onto a reactor scale is briefly considered. A simulation case modelling a conically-shaped debris bed of 200 tonnes of corium in a generic containment geometry is presented. The large-scale simulation shows dryout characteristics similar to those of the earlier small-scale simulations of the experimental beds. The post-dryout behaviour of a multi-dimensionally flooded bed, which may reach steady-states even when local dryout has occurred, is clearly illustrated in the simulation. |
| Key words                        | nuclear reactor, severe accident, dryout heat flux, test facility, core debris, numerical simulation   |